 doi:10.20944/preprints202203.0232.v1

Polymer-coated daikon-based sunlight absorbers for highly efficient interface solar steam generation

Ming Li [a, b, #], Zhenning Zhang [a, b, #], Fan Yang [a, b], Bo Wu [a, b], Jie Yi [a, b], Zhihui Yang [a, b], Yuming Wu [a, b], Weiming Wang [a, b], Shuai Peng [a, b], Jun Xiong [a, b, *], Xue Min [a, b, *]

[1]College of Chemistry and Chemical Engineering, Wuhan Textile University, Wuhan, China

[2]Hubei Key Laboratory of Biomass Fibers and Eco-dyeing & Finishing, Wuhan Textile University, Wuhan, China

[#]These authors contributed equally to this work and should be considered co-first authors

Corresponding authors:

E-mail addresses: jxiong@wtu.edu.cn (Jun Xiong); xmin@wtu.edu.cn (Xue Min).

ABSTRACT: Interface solar steam generation (ISSG) are charming for its applications in desalination and wastewater treatment. Biomass is an attractive substrate for utilizing solar vapor evaporators because of its natural pore structure and water transportability. Polymers like polydopamine (PDA) and polypyrrole (PPy) with broadband spectrum absorption are fascinating in photothermal materials (PTMs). Herein, PDA coated daikon-based (PDA-DK) and PPy coated daikon-based (PPy-DK) PTMs have been exploited for solar steam generation. When polyethylene foam (PEF) was used as an insulating layer to limit heat loss from the PTMs to bulk water, the evaporation rate of PDA-DK and PPy-DK was raised from 0.82 kg m^{-2} h^{-1} and 0.96 kg m^{-2} h^{-1} to 1.50 kg m^{-2} h^{-1} and 1.60 kg m^{-2} h^{-1}, respectively. Meanwhile, the corresponding photothermal conversion efficiency was increased to 89.01% and 98.97%, which was increased by nearly 40% under 1-sun irradiation. In addition, PDA-DK and PPy-DK exhibited remarkable stability for the solar steam generation without significant change through 15 cycles. Furthermore, PDA-DK and PPy-DK could effectively desalt seawater and purify dyeing wastewater. All the results indicate that PDA-DK and PPy-DK have great potential in real-world applications for solar steam generation.

 doi:10.20944/preprints202203.0232.v1

Keywords: Solar steam generation, Photothermal materials, Daikon, Polydopamine, Polypyrrole

1. Introduction

Interface solar steam generation (ISSG) has received much attention for its potential application in seawater desalination and wastewater purification with the huge possibility to solve the worldwide freshwater shortage [1-3]. High efficient solar steam evaporators mainly depend on the exploitation of excellent photothermal materials (PTMs). Superior PTMs should be satisfied the following conditions: broadband light absorption capability, hydrophilic porous structure and excellent stability. The reported PTMs applied to ISSG can be classified into metallic plasmonic materials [4-6], semiconductor materials [7-9], carbon materials [10-13], and so on. For instance, Zhu exploited an Au plasmonic absorber through self-assembly. Due to efficient light absorption, strong field enhancement, and porous structures, the Au plasmonic absorber-based ISSG achieved 90% light to heat conversion efficiency under 4-sun intensity [14]. He fabricated reusable Au plasmonic membranes with broadband solar absorption, high plasmon dissipation losses and fast capillary flow, which resulted in ~85% photothermal efficiency at an illumination power of 10-sun [15]. Yin synthesized the black Ag nanostructures with broadband absorption in the near-infrared and visible spectrum, which were made into thin films for ISSG, and the steam generation efficiency reached as high as 95.25% [16]. However, metallic nanoparticles like Au and Ag are expensive. In addition, most of the nanoparticles such as Fe and Cu are unstable in corrosive media. These disadvantages will restrict their applications in seawater desalination and dye wastewater purification. Many semiconductor-based PTMs have been exploited for ISSG. Shao combined a commercial degreasing cotton, agarose and semiconductor CuS yolk-shell nanocages to fabricate a highly flexible photothermal aerogel, which achieved a water evaporation rate of 1.63 kg m^{-2} h^{-1} with the photothermal efficiency of 94.9% under 1-sun intensity [17]. Yang developed a MoS_2/Bio-carbon foam composite PTM through the hydrothermal self-growth method. Due to the synergistic effect of semiconductor MoS_2 nanosheets and bio-carbon foam,

Preprints (www.preprints.org) | NOT PEER-REVIEWED | Posted: 16 March 2022 doi:10.20944/preprints202203.0232.v1

this PTM could achieve about 96% solar absorption with a water evaporation rate of 1.49 kg m^{-2} h^{-1} under 1-sun illumination [18]. However, the majority of semiconductors are influenced by the narrow absorption band, which limits the semiconductor-based PTM to achieve a high evaporation rate. Carbon-based PTMs are extremely popular among researchers to realize the high evaporation rate because of the broadband absorption band. For instance, Liu used the carbonized upper leaves of rice straw as the light absorber that could attain 89.4% light absorption. The water evaporation rate was 1.2 kg m^{-2} h^{-1} with 75.8% photothermal conversion efficiency [19]. Li fabricated bagasse-based photothermal aerogel, which was consisted of water transporter bagasse-derived cellulose fiber and light absorber carbonized bagasse. This aerogel could absorb about 95% sunlight, which resulted in a water evaporation rate of 1.36 kg m^{-2} h^{-1}. The energy conversion efficiency was 77.34% under 1-sun irradiation [20]. Xu designed a photothermal aerogel with graphene oxide and cellulose fiber from rice straw through the chemical crosslinking method. This photothermal aerogel could absorb about 97% sunlight with a water evaporation rate of 1.37 kg m^{-2} h^{-1} (1 cm high), and the photothermal conversion efficiency was 73.60% under 1-sun intensity [21]. Qu developed a vertically aligned graphene sheet film that could absorb about 93% of the UV, 98% of visible and nearly all of the near-infrared solar illumination. This PTM could realize a water evaporation rate of 1.62 kg m^{-2} h^{-1} and the photothermal conversion efficiency was up to 86.5 % under 1-solar irradiation [22]. In addition, excellent hydrophilicity is necessary for PTMs to improve water transport. However, carbon-based materials are naturally hydrophobic, which need further modification to enhance hydrophilic capacity. Therefore, the complicated preparation process and high cost of carbon-based PTMs restrict their extensive application.

Besides improving the solar absorption capacity of PTMs, reducing heat loss is an important factor in increasing the water evaporation rate. The insulating layer between the bulk water and PTMs can effectively restrain heat loss. For example, Deng exploited an air-laid-paper-based Au nanoparticle film for solar-enabled evaporation. The heat loss from the PTMs to bulk water was effectively restrained by the middle layer of low thermal insulator air-laid paper. The photothermal efficiency of the air-laid-paper-based

Preprints (www.preprints.org) | NOT PEER-REVIEWED | Posted: 16 March 2022 doi:10.20944/preprints202203.0232.v1

Au nanoparticle film was remarkably increased to 77.8% from 47.8% without using air-laid paper as the insulating layer [23]. Chen utilized the carbon foam as the insulating layer the avoid heat loss for high efficient solar vapor generation, which achieved a light to heat efficiency of 85% under 10-sun intensity [24]. Zhu developed the graphene oxide film and polystyrene foam double layer ISSG system. Polystyrene foam can distinctly reduce heat loss. The graphene oxide film as the light absorber acquired 80% photothermal efficiency at 1-sun irradiation [25]. Wang exploited a PEGylated MoS_2-cotton cloth/polystyrene foam double structure. Due to the strong light absorption capacity of PEGylated MoS_2-cotton cloth and marvelous thermal insulation of polystyrene foam, $80.5 \sim 90 \pm 3.5$ % photothermal efficiency was obtained under 1 ~ 5-sun intensity [26]. Therefore, effectively localizing heat fluxes and avoiding heat loss can significantly improve the water evaporation rate and photothermal efficiency.

In addition to restraining heat loss from the PTMs to bulk water, the water transport channel is another key point for achieving a high water evaporation rate. A large supply of water can lead to rapid evaporation from the surface of PTMs. Biomass naturally possesses a hierarchical porous structure and excellent hydrophilic properties to the benefit of both water transport and steam release. Many biomass-based PTMs have been exploited for high efficient solar steam generators [27-30]. Considering that almost all biomass has relatively low sunlight absorption capacity, there are two main methods to prepare biomass-based solar vapor devices: (1) the carbonization method and (2) the surface coating method. A large number of carbonized biomass-based PTMs have been reported. Zhu employed carbonized mushrooms as a solar steam generation device. This ISSG achieved 78% conversion efficiencies under 1-sun irradiation because of the unique natural structure of mushrooms such as porous context and fibrous stipe for water transport [31]. Zhang used the carbonized lotus seedpod as a solar evaporator, which possessed an excellent light absorption ability of ~99%, and resulted in a water evaporation rate of 1.30 kg m^{-2} h^{-1} under 1-sun intensity due to hydrophilic characteristics and interconnected canals [32]. Zhu applied carbonized daikon (DK) as biomass-based PTM. The close-paced pores as photon traps improved

Preprints (www.preprints.org) | NOT PEER-REVIEWED | Posted: 16 March 2022 doi:10.20944/preprints202203.0232.v1

the light absorption ability by nearly 95%. Because of the honeycomb cellular structure and hydrophilic feature, the carbonized DK could attain a water evaporation rate of 1.57 kg m^{-2} h^{-1} with an energy conversion efficiency of 85.9% under 1-sun illumination [33]. However, carbonized biomass like mushroom and DK are friable due to water loss causing them not to be portable, which restrains their widespread applications. Therefore, the surface coating method has received great consideration to design novel biomass-based PTMs at present. Polymers such as polydopamine (PDA) and polypyrrole (PPy) with broadband absorption and remarkable photothermal efficiency have been widely applied to solar steam generation [34,35]. PDA and PPy particles can link with the cellulose of biomass through hydrogen bonding interaction between the N atom of PDA (or PPy) and hydroxyl groups of cellulose to coat on the surface of biomass without obstructing the 3D channel [36]. Due to excellent hydrophilicity, an interconnected pore network and low thermal conductivity of wood, many polymer-coated wood-based PTMs have been reported [37,38]. However, trees grow slowly, and cutting them down in large numbers will damage the environment. DK with a short growth period is almost freely available. DK contains abundant cellulose that can link with PDA (or PPy) through hydrogen bonding interaction. Moreover, DK with honeycomb cellular structure, numerous interconnected channels and outstanding hydrophilic features make them have the possibility to be fabricated polymer-coated biomass-based PTMs for high efficient solar steam generation.

Here, two polymer-coated daikon-based PTMs were exploited for high efficient solar vapor generation. The flow chart of the preparation process was presented in **Fig. 1**. Depending on the close-packed honeycomb cellular structural DK can capture photon and PDA (or PPy) possesses broadband spectrum absorption, the solar absorption capacity of PDA coated daikon-based (PDA-DK) and PPy coated daikon-based (PPy-DK) was 85.63% and 98.12%, respectively. Owning to the polyethylene foam (PEF) can effectively restrain the heat loss from the PTMs to the bulk water, the evaporation rates of PDA-DK (with PEF) and PPy-DK (with PEF) were 1.50 m^{-2} h^{-1} and 1.60 m^{-2} h^{-1}, with the corresponding photothermal conversion efficiency of 89.01% and 98.97% under 1-sun irradiation, respectively. The PDA-DK and PPy-DK presented

Preprints (www.preprints.org) | NOT PEER-REVIEWED | Posted: 16 March 2022 doi:10.20944/preprints202203.0232.v1

outstanding stability that the photothermal efficiency without significant change even after 15 cycles. The simple preparation method makes the PDA-DK and PPy-DK can be scaled fabrication, and indicates that polymer-coated biomass-based PTMs is hopeful as solar to heat agent in vapor generation devices.

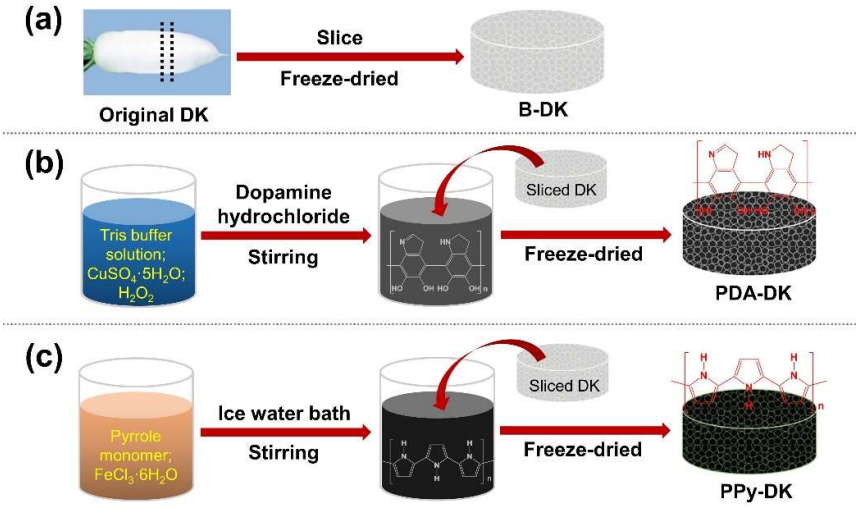

Fig. 1. Schematic illustration of the preparation (a) B-DK; (b) PDA-DK; (c) PPy-DK.

2. Material and methods

2.1 Materials

Fresh DK applied in the experiments was bought from the food market. Dopamine hydrochloride (purity > 98%), pyrrole (purity > 99.7%) and tris(hydroxymethyl) aminomethane hydrochloride (purity > 99%) were purchased from Shanghai Aladdin Co., Ltd., China. $FeCl_3·6H_2O$, $CuSO_4·5H_2O$, H_2O_2 and C_2H_5OH were supplied by Sinopharm Chemical Reagent Co., Ltd., China. All the chemical reagents were utilized without further purification.

2.2 Preparation of blank DK (B-DK), PDA-DK and PPy-DK

The following is the B-DK synthesis method: The B-DK was prepared after washing the fresh DK (height: 1 cm, diameter: 3.5 cm) with deionized water and freeze-drying for 24 hours.

The following is the PDA-DK synthesis method: 0.2 g dopamine hydrochloride was added into the mixture solution, which consisted of Tris buffer solution (100 ml, pH = 8.5), 0.125 g $CuSO_4·5H_2O$ and 0.233 g H_2O_2 with stirring. When the color of the

 doi:10.20944/preprints202203.0232.v1

above mixture changed from blue to dark-brown, the DK (height: 1 cm, diameter: 3.5 cm) was added, and then reacted for 24 hours in a dark and ventilated environment to get black DK. The dark DK was washed with deionized water until no black materials dropped out. The PDA-DK was obtained after freeze-drying the black DK for 24 hours. The black precipitate named PDA was washed through deionized water, and collected by vacuum filtration.

The following is the PPy-DK synthesis method: 0.25 ml pyrrole monomer was added in 150 ml deionized water with ultrasonic for 10 minutes. 50 ml $FeCl_3 \cdot 6H_2O$ (0.075 mol) was dropwise dropped to the above pyrrole solution within 30 minutes under an ice water bath with stirring. Then, the fresh DK (height: 1 cm, diameter: 3.5 cm) was added to the above mixture. Black DK was obtained 6 hours later with stirring. The dark DK was washed with deionized water until no black materials came off. The PDA-DK was gained after freeze-drying the black DK for 24 hours. The black precipitate named PPy was washed through deionized water, and collected by vacuum filtration.

2.3 Characterization

The morphology and ingredient of B-DK, PDA-DK and PPy-DK were confirmed through scanning electron microscopy (SEM), Fourier transform-infrared (FT-IR), X-ray diffraction (XRD) and X-ray photoelectron spectroscopy (XPS). The hydrophily of B-DK, PDA-DK and PPy-DK was evaluated by static contact angles (SCAs). The solar absorption capacity of B-DK, PDA-DK and PPy-DK was estimated by UV-Vis-NIR spectra. Inductively coupled plasma-mass spectroscopy (ICP-MS) was carried out to detect the ion concentration of collection solar water vapor. UV-Vis absorption spectra were applied to evaluate the purification of dyeing wastewater. For the specific model of the instruments, please refer to the Supporting Information (S.I.).

2.4 Solar Steam Generation Experiments

Solar steam generation experiments were carried out at an ambient temperature of around 25 °C with humility of approximately 60%. The height of the sample is 1 cm, and the diameter is 3 cm as illustrated in **Fig. S1**. The samples were put on the surface of the bulk water to perform the solar evaporation experiments in the absence of a PEF

Preprints (www.preprints.org) | NOT PEER-REVIEWED | Posted: 16 March 2022 doi:10.20944/preprints202203.0232.v1

insulating layer as shown in **Fig. S2**a. The samples (height: 1 cm, diameter: 3 cm) were placed on the PEF (height: 2 cm) surface to evaluate the solar evaporation experiments using PEF as an insulating layer as shown in **Fig S2**b. Pumping bulk water to the DK-based PTMs was accomplished by using filter paper. To simulate sunlight, a xenon lamp (Perfect light, CHF500, with standard AM 1.5G spectral optical filter) was used. The mass change of evaporated water was recorded using an electronic balance (RADWAG, 0.0001 g inaccuracy) connected to a computer. All solar vapor generation experiments were performed for 1 hour at a constant 1-sun intensity. An infrared camera (Fluke, TiS60+) was utilized to track the top surface temperature of the PTMs. NaCl (13.37 g), KCl (0.36 g), $MgCl_2$ (1.13 g), $CaCl_2$ (0.58 g) and $MgSO_4$ (1.63 g) were completely dissolved in 500 ml deionized water as seawater for the desalination experiments. Methylene blue solution (20 mg L^{-1}) was used to simulate dyeing wastewater for solar evaporation water purification experiments.

3. Results and discussion

The digital photos of B-DK, PDA-DK and PPy-DK samples were shown in **Fig. 2**a, **2**e and **2**i, respectively. Non-uniform honeycomb cellular structural pores with the size from 50 to 150 μm of B-DK, PDA-DK and PPy-DK were observed as shown in **Fig. 2**b, **2**f and **2**j respectively. The white DK was turned into black after deposition of PDA or PPy. The B-DK had a smooth surface as shown in **Fig. 2**c. The SEM images of PDA-DK revealed that the DK was coated with PDA as exhibited in **Fig. 2**f and **2**g. Meanwhile, the DK was covered by PPy in the PPy-DK as illustrated in **Fig. 2**j and **2**k. The results implied that PDA (or PPy) was loaded on the DK. The energy dispersive X-ray (EDX) spectroscopy demonstrated that B-DK, PDA-DK and PPy-DK mainly contain C, O and N elements as exhibited in **Fig. 2**d, **2**h and **2**l, respectively. PDA-DK also had Cu and S elements, and PPy-DK comprised Fe and Cl elements as shown in **Fig. S3**. This could be attributed to the $CuSO_4$ and $FeCl_3$ as the catalyst to prepare PDA-DA and PPy-DK, respectively. Moreover, Cu, S and Fe, Cl elements could be detected in the PDA-DK and PPy-DK through XPS spectra as shown in **Fig. 3**a.

Preprints (www.preprints.org) | NOT PEER-REVIEWED | Posted: 16 March 2022 doi:10.20944/preprints202203.0232.v1

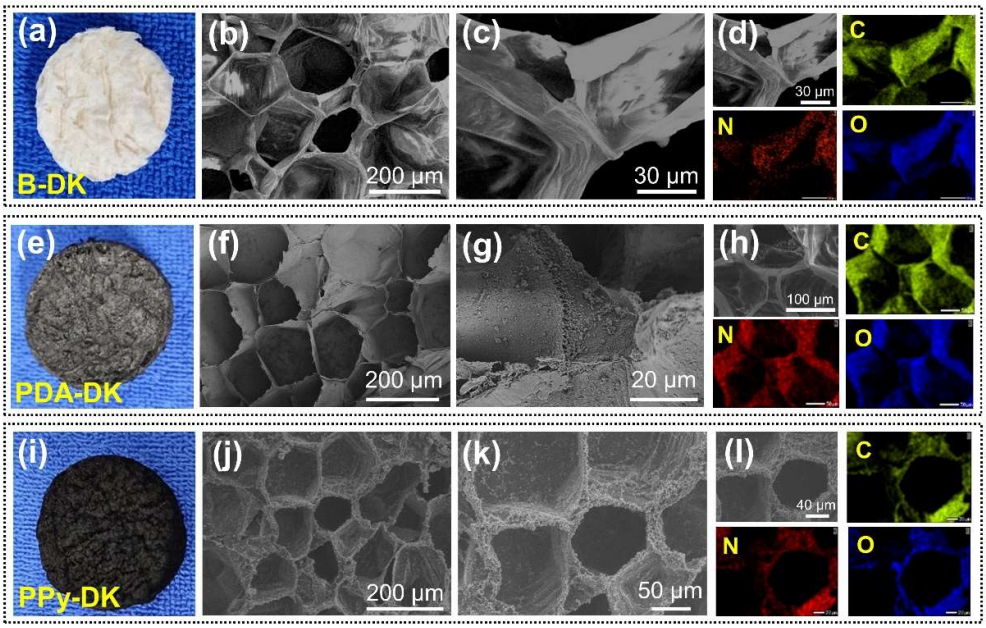

Fig. 2. Photograph and SEM image of B-DK, PDA-DK and PPy-DK: (a) photograph of B-DK; (b–c) SEM images of B-DK under different magnification; (d) element C, N and O mapping images of B-DK; (e) photograph of PDA-DK, (f–g) SEM images of PDA-DK under different magnification; (h) element C, N and O mapping images of PDA-DK; (i) photograph of PPy-DK, (j–k) SEM images of PPy-DK under different magnification; (l) element C, N and O mapping images of PPy-DK.

The prepared B-DK, PDA-DK, PPy-DK, PDA and PPy were ground into power. The samples especially for PDA-DK and PPy-DK was washed with deionized water to remove the Fe^{3+} and Cu^{2+}, respectively. The vacuum dried samples were used for XRD measurement. The peaks at 16° and 22° in the B-DK corresponded to the (1 1 0) and (2 0 0) cellulose diffraction planes, respectively [39,40]. The board peaks at 25.5° and 42.2° matched the PDA (0 0 2) and (1 0 1), respectively [41]. The characteristic peaks at 16°, 22° and 42.2° in the XRD pattern of PDA-DK suggested that PDA was loaded onto the DK as shown in **Fig. 3**a. The XRD pattern of PPy exhibited an amorphous feature of 2θ between 23° and 28° which can be ascribed to the scattering from the PPy chains at the interplanar spacing [42, 43]. The XRD pattern of PPy-DK displayed feature peaks at 16° and 22°, as well as a broad peak ranging between 23° and 28°,

Preprints (www.preprints.org) | NOT PEER-REVIEWED | Posted: 16 March 2022 doi:10.20944/preprints202203.0232.v1

indicating that PPy was coated on the DK as shown in **Fig. 3**b. The FI-IR spectra of B-DK, PDA and PDA-DK were shown in **Fig. 3**c. In comparison to the B-DK, the O-H bond stretching vibration moved from 3415 cm^{-1} to 3443 cm^{-1}, which could be attributed to the hydrogen bonding between the -OH functional groups of lignin and the nitrogen lone pairs of PDA molecules [36]. Simultaneously, the absorption peak at 594 cm^{-1} confirmed the presence of a copolymer composite in PDA-DK [41]. All of the results indicated that PDA was successfully deposited on the DK. The FT-IR characteristic peaks of PPy-DK at 1544 cm^{-1}, 1460 cm^{-1} and 789 cm^{-1} were assigned to the C-C bonds, C-N bonds, and out-of-plane deformation bonds of the pyrrole ring, respectively [44]. Additionally, in comparison to the B-DK, the stretching vibration of the O-H bond was shifted from 3443 cm^{-1} to 3415 cm^{-1}, which could be attributable to the hydrogen bonding interaction between the PPy nitrogen lone pairs and the DK –OH groups [45]. The above results verified that PDA and PPy both coated the surface of DK.

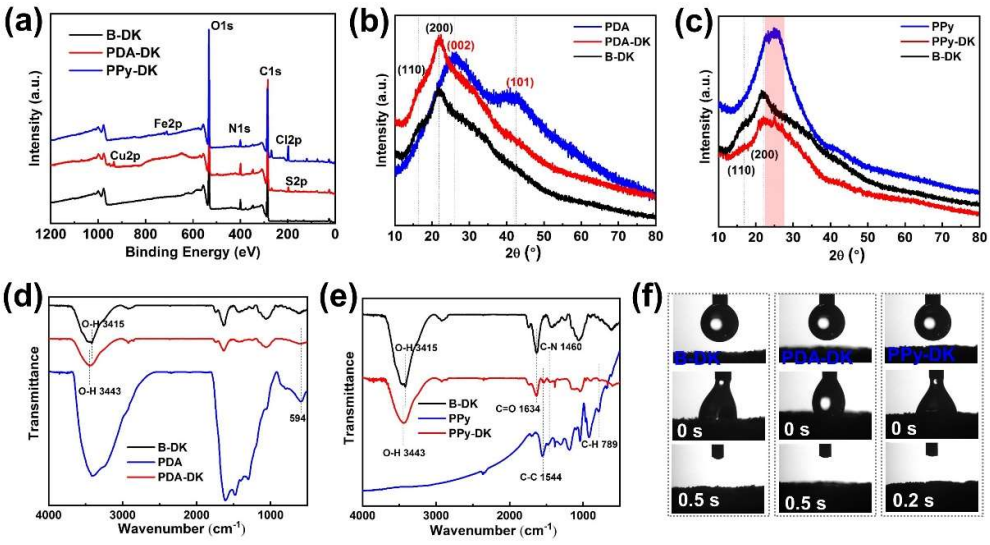

Fig. 3. (a) XPS spectra of B-DK, PDA-DK and PPy-DK; (b) XRD patterns of B-DK, PDA and PDA-DK; (c) XRD patterns of B-DK, PPy and PPy-DK; (d) FT-IR spectra of B-DK, PDA and PDA-DK; (e) FT-IR spectra of B-DK, PPy and PPy-DK; (f) time-lapse snapshots of absorption a water droplet by B-DK, PDA-DK and PPy-DK.

The XPS and SCAs were measured to judge the hydrophilicity of B-DK, PDA-

Preprints (www.preprints.org) | NOT PEER-REVIEWED | Posted: 16 March 2022 doi:10.20944/preprints202203.0232.v1

DK and PPy-DK. The high-resolution spectrum C 1s peaks of B-DK, PDA-DK and PPy-DK around the 286.2 eV and 288.1 eV could be attributed to the C-N^+/C=N and O-C=O respectively, indicating that the DK-based PTMs were hydrophilic as shown in **Fig. S**4 [45]. In addition, as shown in **Fig. 3**f, a water droplet was entirely absorbed by B-DK, PDA-DK and PPy-DK within 0.5 seconds, implying that the BK-based PTMs exhibited superior hydrophilic and water transport properties that are advantageous for solar steam generation.

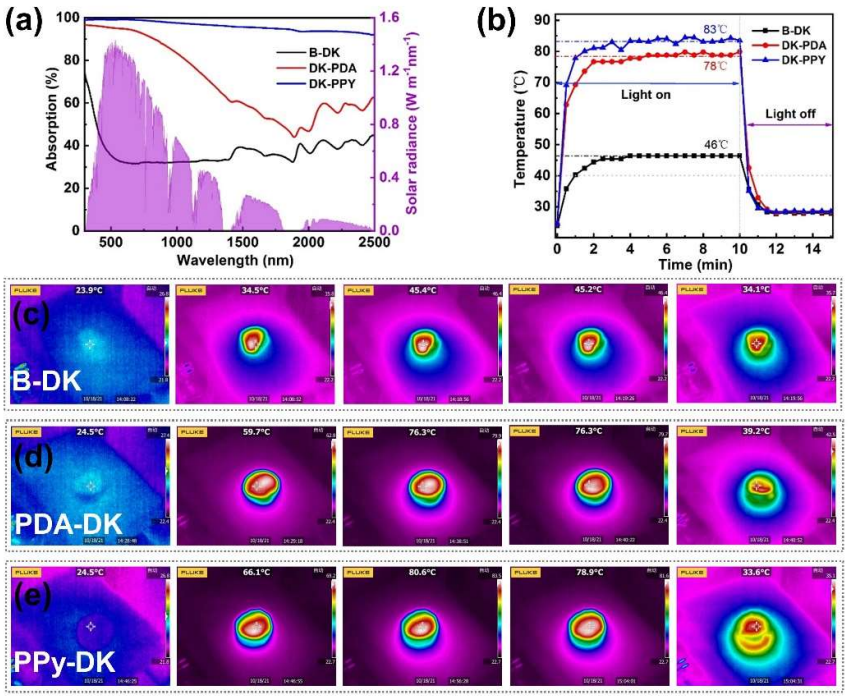

Fig. 4. (a) UV-Vis-NIR spectra of B-DK, PDA-DK and PPy-DK together with solar spectral illumination (AM 1.5G, purple area); (b) time-dependent surface temperatures change of dry B-DK, PDA-DK and PPy-DK under 1-sun irradiation in the air; (c) IR images of dry B-DK under 1-sun intensity in the air for 0, 0.5, 10 minutes and light off for 30 seconds; (c) IR images of dry PDA-DK under 1-sun intensity for 0, 0.5, 10 minutes and light off for 30 seconds; (e) IR images of dry PPy-DK under 1-sun intensity for 0, 0.5, 10 minutes and light off for 30 seconds.

PTMs possessing a broadband sunlight capability is essential to attain high efficient solar steam generation. UV–Vis–NIR spectra were performed to evaluate the

Preprints (www.preprints.org) | NOT PEER-REVIEWED | Posted: 16 March 2022 doi:10.20944/preprints202203.0232.v1

light absorption capabilities of B-DK, PDA-DK and PPy-DK from 300 to 2500 nm as shown in **Fig. 4**a. The light absorption capacity of B-DK, PDA-DK and PPy-DK was 33.13%, 85.63% and 98.11%, respectively. A detailed explanation of the calculation method was explained in S.I. (**Table S1**). The solar absorption ability of PDA-DK (or PPy-DK) was significantly stronger than B-DK, which could be ascribed to the PDA (or PPy) coating on the surface of DK. Meanwhile, the sunlight absorption capacity of PPy-DK was higher than PDA-DK. The UV–Vis–NIR results preliminarily indicated that the photothermal efficiency was PPy-DK > PDA-DK > B-DK.

To assess the light-to-heat capacity further, the top surface temperatures of dry B-DK, PDA-DK, and PPy-DK were monitored using an infrared camera at 1-sun intensity. After 30 seconds of illumination, the top surface temperature of B-DK was elevated to 36.8 °C from 23.9 °C. After two minutes of illumination, the temperature was maintained at 46 °C as shown in **Fig. 4**b. However, the top surface temperatures of PDA-DK and PPy-DK were rapidly increased to 62.8 °C and 69.2 °C from 24.5 °C in the first 30 seconds and maintained at 78 °C and 83 °C after 2 minutes of irradiation as shown in **Fig. 4**b. When the light was turned off for 30 seconds, the top surface temperature of dry B-DK, PDA-DK, and PPy-DK rapidly decreased to 35.7 °C, 42.7 °C, and 35.1 °C, respectively. The infrared images of dry B-DK, PDA-DK and PPy-DK were shown in **Fig. 4**c-**4**e, respectively. PPy-DK has the greatest difference in top surface temperature between light on and off situations. The degree of change in top surface temperature can be used to determine the light-to-heat capability of PTMs. Therefore, the photothermal conversion capacity here is PPy-DK > PDA-DK > B-DK, which coincides with the results of UV-Vis-NIR.

The water evaporation rate and photothermal efficiency of pure water, B-DK (without PEF), PDA-DK (without PEF), PPy-DK (without PEF), B-DK (with PEF), PDA-DK (with PEF), and PPy-DK (with PEF) were investigated under 1-sun intensity. The initial and maximum top surface temperatures of the PTMs are essential according to the photothermal efficiency calculation equation (please refer to the S.I.). The top surface temperature of the PTMs was tracked using an infrared camera. Due to the low density of the DK-based PTMs, they can float on the water surface and can be wetted

 doi:10.20944/preprints202203.0232.v1

due to the strong capillary force. Therefore, the water evaporation rates of B-DK (without PEF), PDA-DK (without PEF), and PPy-DK (without PEF) were determined with the condition of being directly in contact with the bulk water. After 5 minutes of illumination, the top surface temperatures of pure water, B-DK (without PEF), PDA-DK (without PEF), and PPy-DK (without PEF) increased from 22.2 °C, 19.1 °C, 20 °C, and 18.9 °C to 24.7 °C, 28.5 °C, 35.6 °C, and 41.5 °C, respectively, as shown in **Fig. 5**a. After 10 minutes of irradiation, the top surface temperature remained steady, and the average temperature (from 10 to 60 minutes) of pure water, B-DK (without PEF), PDA-DK (without PEF), and PPy-DK (without PEF) was approximately 28 °C, 31 °C, 41 °C, and 43 °C, respectively. The magnitude of the temperature shift suggested that PPy-DK was the best candidate for solar vapor generation. The infrared images of pure water, B-DK (without PEF), PDA-DK (without PEF), and PPy-DK (without PEF) were exhibited in **Fig. S**5. The evaporation rate of pure water, B-DK (without PEF), PDA-DK (without PEF), and PPy-DK (without PEF) was 0.22 kg m^{-2} h^{-1}, 0.25 kg m^{-2} h^{-1}, 0.82 kg m^{-2} h^{-1}, and 0.96 kg m^{-2} h^{-1}, respectively, as shown in **Fig. 5**b. The darkfield evaporation rate of pure water, B-DK (without PEF), PDA-DK (without PEF), and PPy-DK (without PEF) was 0.10 kg m^{-2} h^{-1}, 0.14 kg m^{-2} h^{-1}, 0.11 kg m^{-2} h^{-1}, and 0.12 kg m^{-2} h^{-1}, respectively, as shown in **Fig. S6**. According to the photothermal efficiency equation, the corresponding photothermal efficiency was 8.19%, 7.23%, 49.51% and 58.65%, respectively, as shown in **Fig. 5**f. The low photothermal efficiency could be attributed to heat loss due to direct contact between bulk water and PTMs.

To improve solar vapor generation, PEF (thickness: 2 cm) was applied to the ISSG system as a thermally insulating layer to prevent heat loss from the PTMs to bulk water. Water was pumped to the top surface of PTMs using filter paper. After 5 minutes of irradiation, the top surface temperatures of B-DK (with PEF), PDA-DK (with PEF), and PPy-DK (with PEF) increased from 20.3 °C, 20.9 °C, and 23.1 °C to 30.4 °C, 37.8 °C, and 43.9 °C, respectively. After 10 minutes of illumination, the top surface temperature remained constant. The average temperature (from 10 to 60 minutes) of B-DK (with PEF), PDA-DK (with PEF), and PPy-DK (with PEF) was around 32 °C, 42 °C, and 45 °C, respectively, which was higher than the comparable DK-based PTMs

Preprints (www.preprints.org) | NOT PEER-REVIEWED | Posted: 16 March 2022 doi:10.20944/preprints202203.0232.v1

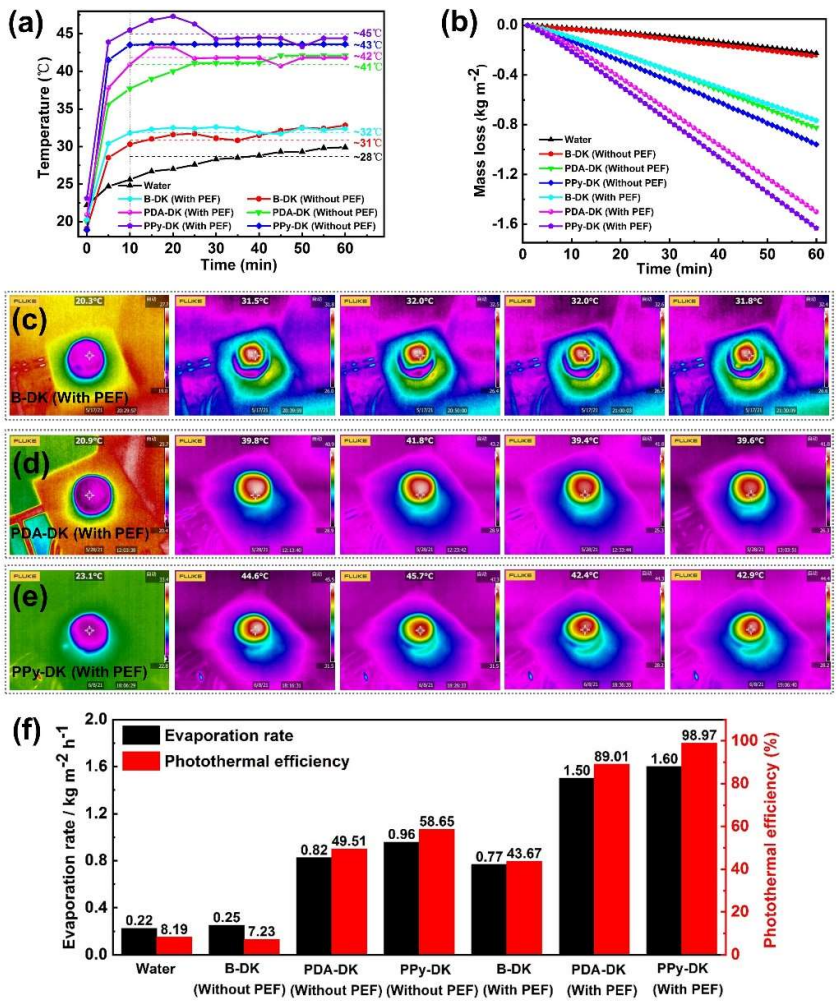

Fig. 5. (a) Time-dependent temperature of the top surface of pure water, B-DK (without PEF), PDA-DK (without PEF), PPy-DK (without PEF), B-DK (with PEF), PDA-DK (with PEF) and PPy-DK (with PEF); (b) time-dependent weight loss of pure water, B-DK (without PEF), PDA-DK (without PEF), PPy-DK (without PEF), B-DK (with PEF), PDA-DK (with PEF) and PPy-DK (with PEF); (c) IR images of B-DK (with PEF); (d) IR images of PDA-DK (with PEF); (e) IR images of PPy-DK (with PEF) at 0, 10, 20, 30 and 60 mins, respectively; (f) water evaporation rate and photothermal efficiency of pure water, B-DK, PDA-DK, PPy-DK with PEF and without PEF.

(without PEF). The results indicated that PEP foam successfully acted as a heat insulating layer. The infrared images of B-DK (with PEF), PDA-DK (with PEF), and PPy-DK (with PEF) were shown in **Fig. 5**c-**5**e. The water evaporates rate of B-DK (with

Preprints (www.preprints.org) | NOT PEER-REVIEWED | Posted: 16 March 2022 doi:10.20944/preprints202203.0232.v1

PEF), PDA-DK (with PEF) and PPy-DK (with PEF) was 0.77 kg m^{-2} h^{-1}, 1.50 kg m^{-2} h^{-1}, and 1.60 kg m^{-2} h^{-1}, respectively. The corresponding dark-field evaporation rate was 0.13 kg m^{-2} h^{-1}, 0.21 kg m^{-2} h^{-1} and 0.17 kg m^{-2} h^{-1}, respectively, as exhibited in **Fig. S6**. Therefore, the photothermal efficiency of B-DK (with PEF), PDA-DK (with PEF) and PPy-DK (with PEF) was 43.67%, 89.01% and 98.97%, respectively. When compared to DK-based PTMs (without PEF), the photothermal efficiency of B-DK (with PEF), PDA-DK (with PEF), and PPy-DK (with PEF) was significantly increased, about 40%. The results indicated that using PEF as a heat insulating layer could significantly reduce heat loss and increase the photothermal efficiency of PTMs.

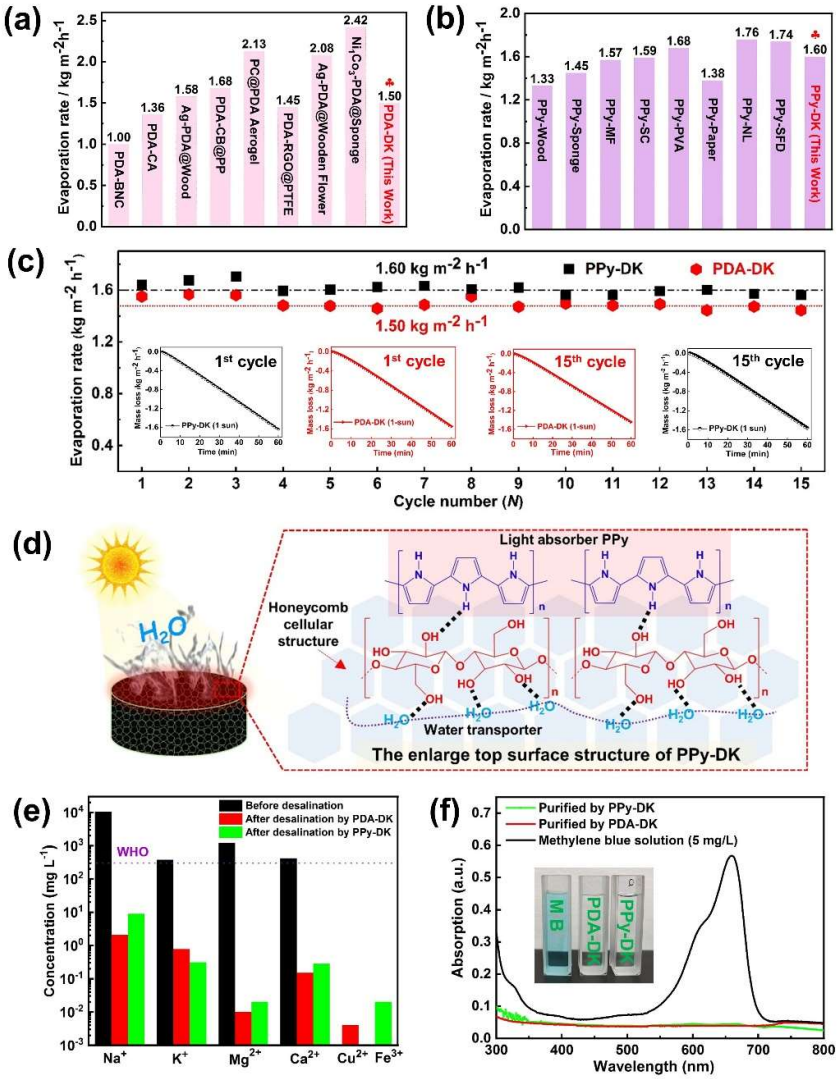

Fig. 6. (a) Comparison of PDA-DK, (b) PPy-DK with previously reported DK-based evaporators (**Table S1**); (c) cycle evaporation performance of PDA-DK and PPy-DK

Preprints (www.preprints.org) | NOT PEER-REVIEWED | Posted: 16 March 2022 doi:10.20944/preprints202203.0232.v1

under 1-sun illumination; (d) scheme of possible mechanism on the ISSG of polymer-based DK (take PPy-DK for example); (e) the concentrations of cations in a simulator seawater sample and after solar thermal desalination by PDA-DK and PPy-DK, respectively; (f) UV-Vis spectra of methyl blue solution (from 20 mg L^{-1} dilute to 5 mg L^{-1}) before and after solar thermal purification by PDA-DK and PPy-DK, respectively (the inserts show the color of the solutions)

The evaporation rates of PDA-DK and PPy-DK were compared to the previously reported PDA-based and PPy-based PTMs as shown in **Fig. 6**a and **6**b, respectively. For the evaporation rates of PDA-based PTMs such as PDA-based bacterial nanocellulose (PDA-BNC; 1.00 kg m^{-2} h^{-1}) [46], PDA-based cellulose aerogel (PDA-CA; 1.36 kg m^{-2} h^{-1}) [47], Ag-PDA@Wood (1.58 kg m^{-2} h^{-1}) [36], PDA-carbon black-based PP non-woven fabric (PDA-CB@PPNWF; 1.68 kg m^{-2} h^{-1}) [48], PDA-RGO-PTFE (1.45 kg m^{-2} h^{-1}) [49], Ag-PDA@Wooden flower (2.08 kg m^{-2} h^{-1}) [50]. For the evaporation rates of PPy-based PTMs such as PPy-Wood (1.33 kg m^{-2} h^{-1}) [38], PPy-Sponge (1.45 kg m^{-2} h^{-1}) [51], PPy-based melamine foam (PPy-MF; 1.57 kg m^{-2} h^{-1}) [52], PPy-based sugarcane (PPy-SC, (1.59 kg m^{-2} h^{-1}) [53], PPy-based polyvinyl alcohol (PPy-PVA; 1.68 kg m^{-2} h^{-1}) [54], PPy-paper (1.38 kg m^{-2} h^{-1}) [55], PPy-based natural latex (1.76 kg m^{-2} h^{-1}) [56], PPy-based sunflower discs (PPy-SFD; 1.74 kg m^{-2} h^{-1}) [57]. The evaporation rate of PDA-DK and PPy-DK were above-average to the previously reported PDA and PPy-based PTMs. In addition, the photothermal efficiency of PDA-DK and PPy-DK remained steady after 15 cycles of 1 hour each under 1-sun irradiation as shown in **Fig. 6**c.

The solar steam generation mechanism of polymer-based DK (for example, PPy-DK) was shown in **Fig. 6**d. To begin, DK includes a large number of hydrophilic groups that facilitate water molecule transport and may deliver sufficient water to the PPy-DK for solar vapor generation. Second, DK features honeycomb cellular structure pores that are advantageous for absorbing sunlight and releasing water vapor [33]. Thirdly, DK is abundant in cellulose, and the hydroxyl groups in cellulose may make hydrogen bonds with bulk water, so disrupting the network of partial hydrogen bonds between

 doi:10.20944/preprints202203.0232.v1

water molecules and lowering the enthalpy of water evaporation [58-60]. Fourthly, the PEF serves as an insulating barrier between the PPy-DK and the bulk water, and minimizing heat loss and enhancing thermal localization [23-25]. Finally, a polymer-coated on the DK is to create a coarse surface that reduces reflection and maximizes solar consumption. Therefore, the high water evaporation rate and photothermal efficiency of polymer-based DK can be achieved.

Outdoor tests were performed to assess the practical application of polymer-coated DK-based PTMs in seawater desalination and dyeing wastewater purification. During the solar steam generation process, the water vapor condensed into droplets that stuck to the spherical glass container as depicted in **Fig. S7**a. Since $FeCl_3 \cdot 6H_2O$ was used to prepare PPy-DK, the ion concentrations of the collected water (Na^+, K^+, Ca^{2+}, Mg^{2+} and Fe^{3+}) were determined using ICP-MS. The ion concentrations (Na^+, K^+, Ca^{2+} and Mg^{2+}) were much lower than those in simulated seawater. The Fe^{3+} ion concentration was 0.04 ppm. as shown in **Fig. 6**e. The collected water fulfilled WHO requirements for drinkable water in terms of positive ion concentrations. (https://www.who.int/water_sanitation_health/publications/dwq-guidelines-4/en/). Because $CuSO_4 \cdot 5H_2O$ was used to fabricate PDA-DK, the ion concentrations of the collected solar desalination water (Na^+, K^+, Ca^{2+}, Mg^{2+} and Cu^{2+}) were determined by ICP-MS and met the WHO drinking water standards [61]. To investigate the efficacy of polymer-coated DK-based PTMs to cleanse dyeing wastewater, solar vapor generation was performed using methyl blue (20 mg L^{-1}) as shown in **Fig. S7**b. UV-Vis absorption spectra were used to determine the quality of the collected water. In comparison to the methyl blue solution (5 mg L^{-1}), the UV-Vis absorbance of the collected water was near zero and the methyl blue peaks vanished, which implied that the obtained water with PDA-DK (or PPy-DK) was clear as shown in **Fig. 6**f. All the results indicated that PDA-DK and PPy-DK were capable of desalinating seawater and purifying dyeing wastewater successfully.

4. Conclusions

In conclusion, two polymer-coated DK-based PTMs (PDA-DK and PPy-DK) have

been exploited for solar steam generation. Due to the synergistic effect of honeycomb cellular structural DK and the broadband spectrum absorption of PDA and PPy, PDA-DK and PPy-DK acquire solar absorption abilities of 85.63% and 98.11% respectively. The evaporation rates of PDA-DK and PPy-DK were increased from 0.82 kg m^{-2} h^{-1} and 0.96 kg m^{-2} h^{-1} to 1.50 kg m^{-2} h^{-1} and 1.60 kg m^{-2} h^{-1}, respectively, when polyethylene foam (PEF) was utilized as an insulating barrier to prevent heat loss from the PTMs to the bulk water. Meanwhile, under 1-sun irradiation, the photothermal conversion efficiency was raised to 89.01% and 98.97%, respectively, an increase of approximately 40%. Furthermore, PDA-DK and PPy-DK demonstrated outstanding stability for solar steam production after 15 cycles with no notable changes. PDA-DK and PPy-DK were also able to desalt seawater and cleanse dyeing effluent. All of the findings suggest that PDA-DK and PPy-DK have huge potential in real-world solar steam generating applications.

Declaration of competing interest

The authors declare that they have no known competing financial interests or personal relationships that could have appeared to influence the work reported in this paper.

Appendix A. Supplementary data

Supplementary data to this article can be found online at

Acknowledgment

The National Natural Science Foundation of China (51203125) and the Hubei Natural Science Foundation (2019CFC905) support this research.

References

[1] V.D. Dao, N.H. Vu, S. Yun, Recent advances and challenges for solar-driven water evaporation system toward applications, Nano Energy 68 (2020) 104324-104341, https://doi.org/10.1016/j.nanoen.2019.104324.

[2] C. Chen, Y. Kuang, L. Hu, Challenges and opportunities for solar evaporation, Joule 3 (2019) 683-718, https://doi.org/10.1016/j.joule.2018.12.023.

[3] P. Tao, G. Ni, C. Song, W. Shang, J. Wu, J. Zhu, G. Chen, T. Deng, Solar-driven interfacial

evaporation, Nat. Energy 3 (2018) 1031-1041, https://doi.org/10.1038/s41560-018-0260-7.

[4] A.R. Mallah, M.N. Mohd Zubir, O.A. Alawi, K.M. Salim Newaz, A.B. Mohamad Badry, Plasmonic nanofluids for high photothermal conversion efficiency in direct absorption solar collectors: fundamentals and applications, Sol. Energy Mater. Sol .Cells 201 (2019) 110084-110114, https://doi.org/10.1016/j.solmat.2019.110084.

[5] O.A. Balitskii, Recent energy targeted applications of localized surface plasmon resonance semiconductor nanocrystals: a mini review, Mater. Today Energy 20 (2021) 100629-100640, https://doi.org/10.1016/j.mtener.2020.100629.

[6] C. Kim, Y. Ryu, D. Shin, A.M. Urbas, K. Kim, Efficient solar steam generation by using metal-versatile hierarchical nanostructures for nickle and gold with aerogel insulator, Appl. Surf. Sci. 517 (2020) 146177-146185, https://doi.org/10.1016/j.apsusc.2020.146177.

[7] F. Tao, Y. Zhang, S. Cao, K. Yin, X. Chang, Y. Lei, R. Fan, L. Dong, Y. Yin, X. Chen, CuS nanoflowers/semipermeable collodion membrane composite for high-efficiency solar vapor generation, Mater. Today Energy 9 (2018) 285-294, https://doi.org/10.1016/j.mtener.2018.06.003.

[8] X. Gao, H. Ren, J. Zhou, R. Du, C. Yin, R. Liu, H. Peng, L. Tong, Z. Liu, J. Zhang, Synthesis of hierarchical graphdiyne-based architecture for efficient solar steam generation, Chem. Mater. 29 (2017) 5777-5781, https://doi.org/10.1021/acs.chemmater.7b01838.

[9] I. Ibrahim, D.H. Seo, A.M. McDonagh, H.K. Shon, L. Tijing, Semiconductor photothermal materials enabling efficient solar steam generation toward desalination and wastewater treatment, Desalination 500 (2021) 114853-114874, https://doi.org/10.1016/j.desal.2020.114853.

[10] V.D. Dao, H.S. Choi, Carbon-based sunlight absorbers in solar-driven steam generation devices, Glob. Chall. 2 (2018) 1700094-1700107, https://doi.org/10.1002/gch2.201700094.

[11] H. Li, Y. He, Y. Hu, X. Wang, Commercially available activated carbon fiber felt enables efficient solar steam generation, ACS Appl. Mater. Interface 10 (2018) 9362-9368, https://doi.org/10.1021/acsami.7b18071.

[12] C. Xiao, W. Liang, Q.M. Hasi, F. Wang, L. Chen, J. He, F. Liu, H. Sun, Z. Zhu, A. Li, Efficient Solar Steam Generation of Carbon Black Incorporated Hyper-Cross-Linked Polymer Composites, ACS Appl. Energy Mater. 3 (2020) 11350-11358, https://doi.org/10.1021/acsaem.0c02290.

[13] Y. Liu, J. Chen, D. Guo, M. Cao, L. Jiang, Floatable, self-cleaning, and carbon-black-based superhydrophobic gauze for the solar evaporation enhancement at the air-water interface, ACS Appl.

Mater. Interfaces 7 (2015) 13645-13652, https://doi.org/10.1021/acsami.5b03435.

[14] Y.T. Lin Zhou, Dengxin Ji, Bin Zhu, Pei Zhang, Jun Xu, Qiaoqiang Gan, Zongfu Yu, Jia Zhu, Self-assembly of highly efficient, broadband plasmonic absorbers for solar steam generation, Sci. Adv. 2 (2016) e1501227-15012234. https://doi.org/10.1126/sciadv.1501227.

[15] X. Wang, Y. He, X. Liu, G. Cheng, J. Zhu, Solar steam generation through bio-inspired interface heating of broadband-absorbing plasmonic membranes, Appl. Energy 195 (2017) 414-425, https://doi.org/10.1016/j.apenergy.2017.03.080.

[16] J. Chen, J. Feng, Z. Li, P. Xu, X. Wang, W. Yin, M. Wang, X. Ge, Y. Yin, Space-confined seeded growth of black silver nanostructures for solar steam generation, Nano Lett. 19 (2019) 400-407, https://doi.org/10.1021/acs.nanolett.8b04157.

[17] X. Wu, M.E. Robson, J.L. Phelps, J.S. Tan, B. Shao, G. Owens, H. Xu, A flexible photothermal cotton-CuS nanocage-agarose aerogel towards portable solar steam generation, Nano Energy 56 (2019) 708-715, https://doi.org/10.1016/j.nanoen.2018.12.008.

[18] X. Zhang, G. Wu, X.C. Yang, MoS2 nanosheet–carbon foam composites for solar steam generation, ACS Appl. Nano Mater. 3 (2020) 9706-9714, https://doi.org/10.1021/acsanm.0c01712.

[19] Q. Fang, T. Li, Z. Chen, H. Lin, P. Wang, F. Liu, Full biomass-derived solar stills for robust and stable evaporation to collect clean water from various water-bearing media, ACS Appl. Mater. Interfaces 11 (2019) 10672-10679, https://doi.org/10.1021/acsami.9b00291.

[20] J. Xiong, Z. Zhang, Y. Liu, J. Yi, Y. Wang, B. Li, W. Wang, S. Peng, X. Min, Y. Gui, M. Li, J. Peng, Full bagasse bio-waste derived 3D photothermal aerogels for high efficient solar steam generation, Cellulose (2021) https://doi.org/10.1007/s10570-021-04323-6.

[21] D.P. Storer, J.L. Phelps, X. Wu, G. Owens, N.I. Khan, H. Xu, Graphene and rice-straw-fiber-based 3D photothermal aerogels for highly efficient solar evaporation, ACS Appl. Mater. Interfaces 12 (2020) 15279-15287, https://doi.org/10.1021/acsami.0c01707.

[22] P. Zhang, J. Li, L. Lv, Y. Zhao, L. Qu, Vertically aligned graphene sheets membrane for highly efficient solar thermal generation of clean water, ACS Nano 11 (2017) 5087-5093, https://doi.org/10.1021/acsnano.7b01965.

[23] Y. Liu, S. Yu, R. Feng, A. Bernard, Y. Liu, Y. Zhang, H. Duan, W. Shang, P. Tao, C. Song, T. Deng, A bioinspired, reusable, paper-based system for high-performance large-scale evaporation, Adv. Mater. 27 (2015) 2768-2774, https://doi.org/10.1002/adma.201500135.

[24] H. Ghasemi, G. Ni, A.M. Marconnet, J. Loomis, S. Yerci, N. Miljkovic, G. Chen, Solar steam generation by heat localization, Nat. Commun. 5 (2014) 4449-4455, https://doi.org/10.1038/ncomms5449.

[25] X. Li, W. Xu, M. Tang, L. Zhou, B. Zhu, S. Zhu, J. Zhu, Graphene oxide-based efficient and scalable solar desalination under one sun with a confined 2D water path, Proc. Natl. Acad. Sci. USA 113 (2016) 13953-13958, https://doi.org/10.1073/pnas.1613031113.

[26] Z. Guo, G. Wang, X. Ming, T. Mei, J. Wang, J. Li, J. Qian, X. Wang, PEGylated self-growth MoS2 on a cotton cloth substrate for high-efficiency solar energy utilization, ACS Appl. Mater. Interfaces 10 (2018) 24583-24589, https://doi.org/10.1021/acsami.8b08019.

[27] I. Ibrahim, V. Bhoopal, D.H. Seo, M. Afsari, H.K. Shon, L.D. Tijing, Biomass-based photothermal materials for interfacial solar steam generation: a review, Mater. Today Energy 21 (2021) 100716-100734, https://doi.org/10.1016/j.mtener.2021.100716.

[28] C. Jia, Y. Li, Z. Yang, G. Chen, Y. Yao, F. Jiang, Y. Kuang, G. Pastel, H. Xie, B. Yang, S. Das, L. Hu, Rich mesostructures derived from natural woods for solar steam generation, Joule 1 (2017) 588-599, https://doi.org/10.1016/j.joule.2017.09.011.

[29] P. Sun, W. Zhang, I. Zada, Y. Zhang, J. Gu, Q. Liu, H. Su, D. Pantelic, B. Jelenkovic, D. Zhang, 3D-structured carbonized sunflower heads for improved energy efficiency in solar steam generation, ACS Appl. Mater. Interfaces 12 (2020) 2171-2179, https://doi.org/10.1021/acsami.9b11738.

[30] Y. Long, S. Huang, H. Yi, J. Chen, J. Wu, Q. Liao, H. Liang, H. Cui, S. Ruan, Y.J. Zeng, Carrot-inspired solar thermal evaporator, J Mater. Chem. A 7 (2019) 26911-26916, https://doi.org/10.1039/c9ta08754k.

[31] N. Xu, X. Hu, W. Xu, X. Li, L. Zhou, S. Zhu, J. Zhu, Mushrooms as efficient solar steam-generation devices, Adv. Mater. 29 (2017) 1606762-1606766, https://doi.org/10.1002/adma.201606762.

[32] J. Fang, J. Liu, J. Gu, Q. Liu, W. Zhang, H. Su, D. Zhang, Hierarchical porous carbonized lotus seedpods for highly efficient solar steam generation, Chem. Mater. 30 (2018) 6217-6221, https://doi.org/10.1021/acs.chemmater.8b01702.

[33] M. Zhu, J. Yu, C. Ma, C. Zhang, D. Wu, H. Zhu, Carbonized daikon for high efficient solar steam generation, Sol. Energy Mater. Sol. Cells 191 (2019) 83-90, https://doi.org/10.1016/j.solmat.2018.11.015.

[34] Y. Li, J. Fan, R. Wang, W. Shou, L. Wang, Y. Liu, 3D tree-shaped hierarchical flax fabric for highly efficient solar steam generation, J Mater. Chem. A 9 (2021) 2248-2258, https://doi.org/10.1039/d0ta09570b.

[35] J.T. Wang, J.L. Hong, Effect of folding on 3D photothermal cones with efficient solar-driven water evaporation, Appl. Ther. Eng. 178 (2020) 115636-115644, https://doi.org/10.1016/j.applthermaleng.2020.115636.

[36] J. Yang, Y. Chen, X. Jia, Y. Li, S. Wang, H. Song, Wood-based solar interface evaporation device with self-desalting and high antibacterial activity for efficient solar steam generation, ACS Appl. Mater. Interfaces 12 (2020) 47029-47037, https://doi.org/10.1021/acsami.0c14068.

[37] X. Wu, G.Y. Chen, W. Zhang, X. Liu, H. Xu, A plant-transpiration-process-inspired strategy for highly efficient solar evaporation, Adv. Sustain. Syst. 1 (2017) 1700046-1700052, https://doi.org/10.1002/adsu.201700046.

[38] W. Huang, G. Hu, C. Tian, X. Wang, J. Tu, Y. Cao, K. Zhang, Nature-inspired salt resistant polypyrrole–wood for highly efficient solar steam generation, Sustain. Energy Fuels 3 (2019) 3000-3008, https://doi.org/10.1039/c9se00163h.

[39] Y.A. Rodriguez-Restrepo, C.M.R. Rocha, J.A. Teixeira, C.E. Orrego, Valorization of passion fruit stalk by the preparation of cellulose nanofibers and immobilization of trypsin, Fiber. Polym. 21 (2020) 2807-2816, https://doi.org/10.1007/s12221-020-1342-2.

[40] M. Mohiuddin, K.K. Sadasivuni, S. Mun, J. Kim, Flexible cellulose acetate/graphene blueprints for vibrotactile actuator, RSC Adv. 5 (2015) 34432-34438, https://doi.org/10.1039/c5ra03043a.

[41] M. Sivakumar, K. Pandi, S.M. Chen, An effective electrocatalytic oxidation of 4-Aminoantipyrine in the biological sample using polydopamine@polypyrrole copolymer modified glassy carbon electrode, J Polym. Res. 28 (2021) 266-273, https://doi.org/10.1007/s10965-021-02598-8.

[42] K. Malook, H. Khan, M. Shah, H. Ihsan Ul, Synthesis, characterization and electrical properties of polypyrrole/V2O5 composites, Korean J Chem. Eng. 35 (2017) 12-19, https://doi.org/10.1007/s11814-017-0263-2.

[43] S.P. Raghunathan, S. Narayanan, A.C. Poulose, R. Joseph, Flexible regenerated cellulose/polypyrrole composite films with enhanced dielectric properties, Carbohydr. Polym. 157 (2017) 1024-1032, https://doi.org/10.1016/j.carbpol.2016.10.065.

[44] C.S. Priya, G. Velraj, Synthesis and characterization of nano and micro copper doped conducting polymer, Mater. Lett. 77 (2012) 29-31, https://doi.org/10.1016/j.matlet.2012.02.112.

[45] Z. Wang, Y. Yan, X. Shen, C. Jin, Q. Sun, H. Li, A wood–polypyrrole composite as a photothermal conversion device for solar evaporation enhancement, J Mater. Chem. A 7 (2019) 20706-20712, https://doi.org/10.1039/c9ta04914b.

[46] X. Wu, S. Cao, D. Ghim, Q. Jiang, S. Singamaneni, Y.S. Jun, A thermally engineered polydopamine and bacterial nanocellulose bilayer membrane for photothermal membrane distillation with bactericidal capability, Nano Energy 79 (2021) 105353-105363, https://doi.org/10.1016/j.nanoen.2020.105353.

[47] Y. Zou, J. Zhao, J. Zhu, X. Guo, P. Chen, G. Duan, X. Liu, Y. Li, A mussel-inspired polydopamine-filled cellulose aerogel for solar-enabled water remediation, ACS Appl. Mater. Interfaces 13 (2021) 7617-7624, https://doi.org/10.1021/acsami.0c22584.

[48] S. Sun, B. Sun, Y. Wang, M. Fordjour Antwi-Afari, H.-Y. Mi, Z. Guo, C. Liu, C. Shen, Carbon black and polydopamine modified non-woven fabric enabling efficient solar steam generation towards seawater desalination and wastewater purification, Sep. Purif. Technol. 278 (2021) 119621-119631, https://doi.org/10.1016/j.seppur.2021.119621.

[49] B. Bai, X. Yang, R. Tian, X. Wang, H. Wang, A high efficiency solar steam generation system with using residual heat to enhance steam escape, Desalination 491 (2020) 114382-114391, https://doi.org/10.1016/j.desal.2020.114382.

[50] S. Chen, Z. Sun, W. Xiang, C. Shen, Z. Wang, X. Jia, J. Sun, C.J. Liu, Plasmonic wooden flower for highly efficient solar vapor generation, Nano Energy 76 (2020) 104998-105007, https://doi.org/10.1016/j.nanoen.2020.104998.

[51] Y. Fan, W. Bai, P. Mu, Y. Su, Z. Zhu, H. Sun, W. Liang, A. Li, Conductively monolithic polypyrrole 3-D porous architecture with micron-sized channels as superior salt-resistant solar steam generators, Sol. Energy Mater. Sol. Cells 206 (2020) 110347-110355, https://doi.org/10.1016/j.solmat.2019.110347.

[52] C. Li, D. Jiang, B. Huo, M. Ding, C. Huang, D. Jia, H. Li, C.Y. Liu, J. Liu, Scalable and robust bilayer polymer foams for highly efficient and stable solar desalination, Nano Energy 60 (2019) 841-849, https://doi.org/10.1016/j.nanoen.2019.03.087.

[53] C. Xiao, L. Chen, P. Mu, J. Jia, H. Sun, Z. Zhu, W. Liang, A. Li, Sugarcan-based photothermal

materials for efficient solar steam generation, ChemistrySelect 4 (2019) 7891-7895, https://doi.org/10.1002/slct.201901889.

[54] B. Wen, X. Zhang, Y. Yan, Y. Huang, S. Lin, Y. Zhu, Z. Wang, B. Zhou, S. Yang, J. Liu, Tailoring polypyrrole-based Janus aerogel for efficient and stable solar steam generation, Desalination 516 (2021) 115228-115237, https://doi.org/10.1016/j.desal.2021.115228.

[55] X. Wang, Q. Liu, S. Wu, B. Xu, H. Xu, Multilayer polypyrrole nanosheets with self-organized surface structures for flexible and efficient solar-thermal energy conversion, Adv. Mater. 31 (2019) e1807716-e1807714, https://doi.org/10.1002/adma.201807716.

[56] Y. Xu, J. Wang, F. Yu, Z. Guo, H. Cheng, J. Yin, L. Yan, X. Wang, Flexible and efficient solar thermal generators based on polypyrrole coated natural latex foam for multimedia purification, ACS Sustainable Chem. Eng. 8 (2020) 12053-12062, https://doi.org/10.1021/acssuschemeng.0c03164.

[57] Y. Chen, G. Zhao, L. Ren, H. Yang, X. Xiao, W. Xu, Blackbody-inspired array structural polypyrrole-sunflower disc with extremely high light absorption for efficient photothermal evaporation, ACS Appl. Mater. Interfaces 12 (2020) 46653-46660, https://doi.org/10.1021/acsami.0c11549.

[58] H. Bai, N. Liu, L. Hao, P. He, C. Ma, R. Niu, J. Gong, T. Tang, Self-floating efficient solar steam generators constructed using super-hydrophilic N,O dual-doped carbon foams from waste polyester, Energy Environ. Mater. 0 (2021) 1-10, https://doi.org/10.1002/eem2.12235.

[59] Z. Sun, W. Li, W. Song, L. Zhang, Z. Wang, A high-efficiency solar desalination evaporator composite of corn stalk, mcnts and TiO2: ultra-fast capillary water moisture transportation and porous bio-tissue multi-layer filtration, J Mater. Chem. A 8 (2020) 349-357, https://doi.org/10.1039/c9ta10898j.

[60] J. Xiong, Z. Zhang, J. Yi, B. Li, X. Wang, Y. Wang, W. Wang, S. Peng, X. Min, M. Li, J. Peng, Hierarchical MnO2 nanosheets grown on cotton fabric as a flexible and washable solar evaporator for seawater desalination, ACS Appl. Nano Mater. (2021) https://doi.org/10.1021/acsanm.1c03089.

[61] S. Raymond-Whish, L.P. Mayer, T. O'Neal, A. Martinez, M.A. Sellers, P.J. Christian, S.L. Marion, C. Begay, C.R. Propper, P.B. Hoyer, C.A. Dyer, Drinking water with uranium below the U.S. EPA water standard causes estrogen receptor-dependent responses in female mice, Environ. Health Perspect. 115 (2007) 1711-1716, https://doi.org/10.1289/ehp.9910.

Preprints (www.preprints.org) | NOT PEER-REVIEWED | Posted: 16 March 2022 doi:10.20944/preprints202203.0232.v1

Graphical Abstract